J Appl Physiol 98: 672–679, 2005.
First published September 24, 2004; doi:10.1152/japplphysiol.00619.2004.

Mechanical interactions between collagen and proteoglycans: implications for the stability of lung tissue

Francisco S. A. Cavalcante,[1–3] Satoru Ito,[2] Kelly Brewer,[2] Hiroaki Sakai,[2] Adriano M. Alencar,[2] Murilo P. Almeida,[3] José S. Andrade, Jr.,[3] Arnab Majumdar,[2] Edward P. Ingenito,[4] and Béla Suki[2]

[1]*Department of Física e Química, Universidade Estadual do Ceará, Fortaleza;* [2]*Department of Biomedical Engineering, Boston University, Boston;* [3]*Department of Física, Universidade Federal do Ceará, Fortaleza, Ceará, Brazil; and* [4]*Brigham and Women's Hospital, Harvard Medical School, Boston, Massachusetts*

Submitted 18 June 2004; accepted in final form 23 August 2004

Cavalcante, Francisco S. A., Satoru Ito, Kelly Brewer, Hiroaki Sakai, Adriano M. Alencar, Murilo P. Almeida, José S. Andrade, Jr., Arnab Majumdar, Edward P. Ingenito, and Béla Suki. Mechanical interactions between collagen and proteoglycans: implications for the stability of lung tissue. *J Appl Physiol* 98: 672–679, 2005. First published September 24, 2004; doi:10.1152/japplphysiol.00619.2004.—Collagen and elastin are thought to dominate the elasticity of the connective tissue including lung parenchyma. The glycosaminoglycans on the proteoglycans may also play a role because osmolarity of interstitial fluid can alter the repulsive forces on the negatively charged glycosaminoglycans, allowing them to collapse or inflate, which can affect the stretching and folding pattern of the fibers. Hence, we hypothesized that the elasticity of lung tissue arises primarily from *1*) the topology of the collagen-elastin network and *2*) the mechanical interaction between proteoglycans and fibers. We measured the quasi-static, uniaxial stress-strain curves of lung tissue sheets in hypotonic, normal, and hypertonic solutions. We found that the stress-strain curve was sensitive to osmolarity, but this sensitivity decreased after proteoglycan digestion. Images of immunofluorescently labeled collagen networks showed that the fibers follow the alveolar walls that form a hexagonal-like structure. Despite the large heterogeneity, the aspect ratio of the hexagons at 30% uniaxial strain increased linearly with osmolarity. We developed a two-dimensional hexagonal network model of the alveolar structure incorporating the mechanical properties of the collagen-elastin fibers and their interaction with proteoglycans. The model accounted for the stress-strain curves observed under all experimental conditions. The model also predicted how aspect ratio changed with osmolarity and strain, which allowed us to estimate the Young's modulus of a single alveolar wall and a collagen fiber. We therefore identify a novel and important role for the proteoglycans: they stabilize the collagen-elastin network of connective tissues and contribute to lung elasticity and alveolar stability at low to medium lung volumes.

glycosaminoglycans; stress-strain; stiffness; fluorescent imaging; network

ABNORMAL ELASTICITY OF LUNG tissue has a major impact on the clinical progression and outcome of many lung diseases including respiratory distress syndrome (14), asthma (16), and emphysema (17). However, very little is known about how alterations in the molecular constituents of the connective tissue of the lung affect its macroscopic mechanical properties.

The three primary load-bearing components of lung tissue are elastin, collagen, and proteoglycans. Elastin is composed of flexible cross-linked polypeptides and has a linear stress-strain relation up to 200% strain (12). Collagen has a more organized structure with both crystalline and amorphous phases (13) and exhibits a highly nonlinear stress-strain curve (12, 35). Although the collagen and elastin fibers fold under compression, the proteoglycan aggregates that surround these fibers in the interstitium can resist compression and shear (4). The proteoglycans consists of glycosaminoglycans (GAGs), which are long unbranched carbohydrate chains linked to a protein core. The molecular mechanism of the compressibility of proteoglycans originates from the properties of the GAGs, which contain negatively charged sulfate and carboxyl groups (except the hyaluronic acid) that are closely packed and can generate large electrostatic repulsive forces (4). The prevailing concept is that elastin and collagen fibers dominate elasticity of the connective tissue (12) including lung parenchyma (21, 32, 38). However, the interactions among these molecular constituents of the connective tissue and how they affect lung function is not well understood.

Microscopic images of the parenchyma show that the alveoli, the small gas-exchanging sacs of the lung, are arranged in a hexagonal-like structure (24, 33, 34). Hexagonal networks without preexisting stress (prestress) are unstable because during shear or uniaxial deformations the hexagons collapse (34). During uniform volumetric stretching, the alveoli in the intact lung are stabilized by prestress (34) and surfactant at the air-liquid interface (20). In excised tissue strips, these mechanisms are absent and hence the tissue strips should be unstable under uniaxial stretch. However, uniaxial loading of tissue strips shows that the Young's modulus in fact increases with strain (21, 38). Thus there must be some mechanisms that stabilize the fiber network. We hypothesized that the electrostatically charged network of proteoglycans in which the collagen and elastin fibers are embedded resists the folding of the fibers and hence stabilizes the alveolar structure. To test this hypothesis, we measured the stress-strain curves of normal lung tissue strips under conditions that increase or decrease the compressibility of the proteoglycan aggregates. This can be achieved by controlling the ionic strength of the tissue bath. For example, when the concentration of positive ions is increased, the repulsive forces of the negative charges on the GAGs along the proteoglycans are "screened" and the proteoglycans collapse (4) and decrease their resistance to deformation, which should result in a "softer" stress-strain curve. To quantify this elastic resistance against folding, the stability of the structure was assessed by measuring the macroscopic

Address for reprint requests and other correspondence: B. Suki, Dept. of Biomedical Engineering, Boston Univ., 44 Cummington St., Boston, MA 02215 (E-mail: bsuki@bu.edu).

The costs of publication of this article were defrayed in part by the payment of page charges. The article must therefore be hereby marked "*advertisement*" in accordance with 18 U.S.C. Section 1734 solely to indicate this fact.

stress-strain curve and imaging the deformation of individual alveoli while altering the osmolarity of the bath. To interpret the results, we propose a new microscopic model that accounts for mechanical interaction between the fibers and the proteoglycans.

METHODS

Mechanical measurements. Lungs were obtained from seven healthy male Sprague-Dawley rats weighing between 280 and 350 g. The protocol was approved by the Boston University and Harvard Medical School Animal Care and Use Committees. The animals were killed by intraperitoneal injection of pentobarbital sodium and xylazine. The lungs were removed, degassed in a vacuum chamber, and stored for ~24 h in phosphate-buffered saline (PBS). A cannula was inserted into the main bronchus, and the degassed lobe was inflated with 50 ml/kg of 2% agarose solution at 55°C. The agarose was allowed to gel at room temperature, causing the lung to become stiffer and facilitating slicing with a vibratome. Tissue strips of 5 × 5 mm in length and width and ~0.4 mm in thickness measured by a caliper were cut from subpleural regions excluding the larger airways. The samples were washed in PBS at 55°C to remove the agarose. One sample per lung was used to measure the stress-strain curve, and the remaining two to three strips were used for imaging. The sample was fixed by cyanoacrylate glue to small metal plates attached to straight steel wires. The assembly was placed in a plastic tissue bath containing PBS with one wire attached to a force transducer and the other to a displacement generator.

The displacement generator was a servo-controlled lever arm with a resolution of 1 μm (series 308B, Cambridge Technologies) driven by a computer. The force was measured by a force transducer (model 400A, Cambridge Technologies), which had a resolution of 100 μg and compliance of 1 μm/g. The setup was aligned and calibrated as previously (38). The initial length of the sample was established by measuring the largest length before force was first detected. The sample was stretched uniaxially at a rate of 1%/s up to 30% strain, whereas the displacement and force signals were low-pass filtered at 15 Hz and sampled at 50 Hz. Stress (σ) and strain (ϵ) were calculated as the force normalized by the cross-sectional area and change in length divided by the initial length, respectively.

The first measurement was performed in normal saline solution (0.15 M) followed by measurements in either hypotonic (0.05 M) or hypertonic (0.45 M) saline in random order. We found that after a change of the solution, the stress-strain curves reached equilibrium within 30 min, hence the measurements were separated by 45 min. In three additional strips, after the stress-strain measurements, the GAGs were also digested (26). The strips were first rinsed in cold PBS and placed in a 50-ml sterile conical polypropylene test tube. Each strip was incubated in 10 ml of 0.4% (wt/vol) α-amylase (Sigma, St. Louis, MO) dissolved in 0.22 M sodium phosphate buffer (pH 5.4). Samples were placed in a mechanical shaker at 25°C for 18 h, then removed and rinsed twice in PBS. The stress-strain curves of the samples were then determined as described above.

Imaging. To label collagen or elastin, monoclonal anti-collagen type I and anti-elastin antibodies (Sigma) at concentrations of 7.4 and 10 mg/ml were diluted 1:2,000 and 1:5,000, respectively, with PBS. Samples were immersed into 800 μl of diluted primary antibodies and incubated at 37°C for 1 h. Samples were washed four times in 1 ml of PBS at 20-min intervals, immersed in 800 μl of anti-mouse IgG FITC conjugate (Sigma) at a concentration of 100 μg/ml, and incubated at 37°C for 1 h. Samples were washed again four times in 1 ml of PBS at 20-min intervals. A negative control was carried out in which samples were immersed in the secondary antibody without the primary antibody.

The same setup was used as for the mechanical measurements. One end of the sample was glued to the coverslip and the other to a metal plate connected to the lever arm. The apparatus was fit atop an inverted fluorescent microscope (Zeiss Axiovert 100) with the sample above the objective. The lever arm stretched the sample to a predefined strain, and the sample was left at that strain for 5 min to gain equilibrium. Paired images of ~6–8 regions per strain were captured by use of a charge-coupled device camera at both $\epsilon = 0$ and $\epsilon = 0.3$. A total of 12 samples was analyzed from collagen-labeled and 12 from elastin-labeled tissue with 8 samples imaged in normal (0.15 M), 8 in hypotonic (0.05 M), and 8 in hypertonic (0.45 M) saline.

Numerical model. The elastic behavior of the tissue sheet was modeled by using a two-dimensional network of nonlinearly elastic springs joined by pin joints. Each spring represented the combined mechanical behavior of elastin and collagen fibers within the alveolar wall with a second-order force-length relationship that can be obtained as the derivative of the elastic energy of the spring (E_s) with respect to the spring displacement relative to its resting length (Δl):

$$E_s = \frac{1}{2} k \Delta l^2 + \frac{1}{3} b \Delta l^3 \quad (1)$$

where k is the linear spring constant and b is the nonlinear spring constant. The parameter b accounts for the nonlinearly elastic collagen, whereas k includes contributions from both collagen and elastin.

The springs were arranged in a two-dimensional hexagonal lattice. The nodes of the hexagons along the top and bottom of the network were fixed (see below). Without prestress, hexagons far from the fixed boundary are unstable because they collapses under uniaxial or shear deformation. This instability arises from the fact that the line elements are joined by pin joints allowing them to freely rotate. The Young's modulus of such systems vanishes because the springs do not experience stretching until they are aligned with the strain. To stabilize the network, we assumed that the springs are not free to rotate. This constraint was implemented by introducing a term in the total elastic energy of the system that is a function of the change in the angle between two interconnected springs:

$$E_a = \frac{1}{2} r \Delta\theta^2 \quad (2)$$

where the subscript a indicates that this term accounts for angular contribution, r gives the magnitude of this contribution, also called bond-bending constant (2), and $\Delta\theta$ is the change in angle relative to the resting angle.

We constructed five random hexagonal networks consisting of 527 springs and 169 hexagonal unit cells. To implement heterogeneity similar to that observed in the tissue, we first created a symmetrical network with line elements of unit length and 120° resting angle. Next, the nodes (except those at the top and bottom) were randomly displaced, and each hexagon was randomly twisted. To increase heterogeneity measured by the standard deviation (SD) of the aspect ratio of the hexagons, the procedure was repeated 2–10 times depending on the amount of randomness needed. The lengths and angles in the final configuration were assigned as the new initial lengths and resting angles, respectively, which guaranteed that the total potential energy of the network was zero in the undeformed state. A specified ϵ was then applied by moving the node positions of the top border. The nodes along the top and bottom borders were then kept fixed, whereas the remaining nodes were allowed to move. The equilibrium configuration corresponding to the minimum energy calculated by using *Eqs. 1* and *2* summed for all springs and nodes was obtained by applying a variant of the simulated annealing technique (18). We first calculated the local equilibrium position of each node and moved the node in the direction of its equilibrium with a small amount proportional to the local force (36). If the change in total energy (ΔE) was negative, the configuration was accepted. For $\Delta E > 0$, the new configuration was accepted with a probability $P = \exp(-\Delta E/T)$, where T is a control parameter. These steps were repeated until a convergence criterion was reached (i.e., $\Delta E/E$ remained lower than 10^{-7} for 20 consecutive iterations) and T was reduced according to a predefined scheme. To construct the stress-strain curve of the model, the

network was stretched in steps of $\epsilon = 0.05$ and σ was calculated by numerically differentiating the total energy. Specifically, for every ϵ, the total energy was first calculated, the network was further stretched uniaxially by 0.001%, the corresponding energy was calculated, and σ was obtained as the difference between the energies normalized by the strain.

RESULTS

Experimental results. Figure 1 shows the mean and SD of the stress-strain curves in three solutions. In hypotonic solution the stress shifted to the left, increasing the stiffness, whereas in hypertonic solution the stress shifted to the right. The mean stress significantly depended on both the solution ($P < 0.005$) and strain ($P < 0.0001$), and there was an interaction between solution and strain ($P < 0.001$; 2-way repeated-measures ANOVA). The effect of GAG digestion in the three additional samples was to reduce the stress in normal saline on average by 20%. We further evaluated the effects of digestion by calculating the sensitivity of stress to ionic concentration, defined as the difference between the stresses in hypotonic and hypertonic solutions normalized by the stress in normal saline. Despite the large interindividual variability, at $\epsilon = 0.05$, the sensitivities were ~6–10 times higher in control than after digestion with amylase. The sensitivities decreased with ϵ, but they were still 2–3 higher before than after digestion at $\epsilon = 0.2$.

A typical image of parenchymal tissue slices labeled for collagen in normal solution at $\epsilon = 0$ is shown in Fig. 2*A*. The most noticeable feature is the hexagonal-like pattern of the unit cells of the alveolar structure. The diameters of the unit cells ranged from 40 to 100 μm, suggesting that the fibers contour the alveoli. The means ± SD of the diameters for collagen- and elastin-labeled tissues were 86 ± 23 and 80 ± 21 μm, respectively, not significantly different from each other. After stretching, the unit cells became ellipsoidal in shape. Figure 2*B* shows the alveolar structure from Fig. 2*A* at uniaxial strain of $\epsilon = 0.3$ in the vertical direction. The three segments identified as *1*, *2*, and *3* demonstrate a considerable amount of heterogeneity in their stretching and folding pattern. For example, *segment 1* undergoes 14% stretching and virtually no change in orientation, whereas *segment 2* stretches 11% and folds by 15% toward the direction of strain. In contrast, after stretching, *segment 3* becomes compressed by 3% and folds 7% of its original angle out of the direction of the macroscopic strain. To quantify the shape distortion, we measured the aspect ratio (Ar) of the alveolar structure, defined as the ratio of the diameter of the unit cell in the direction of macroscopic strain ϵ to the diameter perpendicular to the strain. For the middle unit cell that contains *sides 1* and *2*, Ar increased from 1.25 (Fig. 2*A*) to 1.37 (Fig. 2*B*), whereas ϵ increased from 0 to 0.3. Elastin-labeled images showed a similar pattern (not shown).

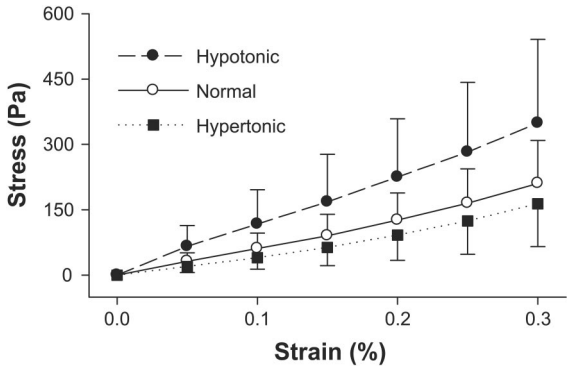

Fig. 1. Means ± SD of stress-strain curves in a population of 7 lung tissue sheets in normal (0.15 M), hypertonic (0.45 M), and hypotonic (0.05 M) saline.

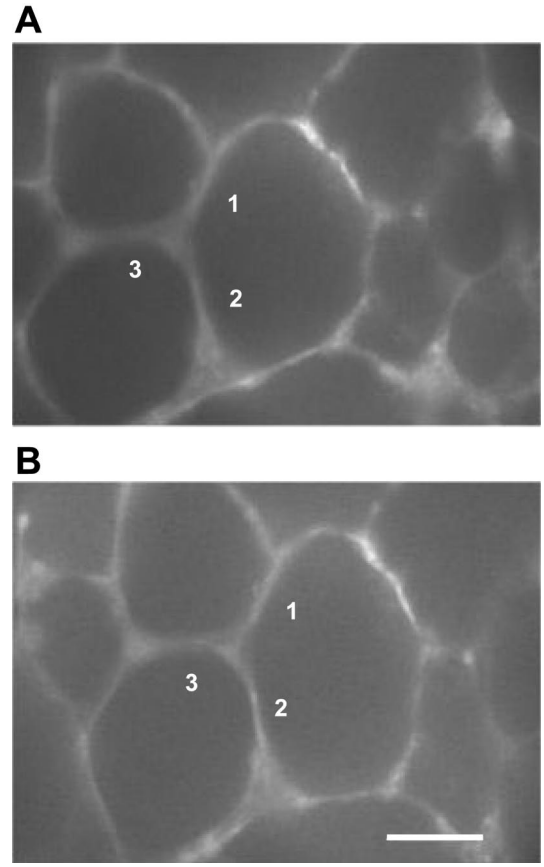

Fig. 2. Immunofluorescently labeled collagen network (white) of lung tissue sheets in normal solution at 0% (*A*) and 30% (*B*) macroscopic strain in the vertical direction. The numbers *1*, *2*, and *3* label the same alveolar walls before and after stretching. Bar represents 50 μm.

The statistics of Ar at zero strain for collagen and elastin were not significantly different from unity and from each other. The Ar highly depended on strain (2-way ANOVA; $P < 0.0001$), and the Ar of collagen was not different from that of elastin. Thus, at this magnification, no features of the alveoli were different for collagen and elastin. Consequently, all features measured separately on the collagen- and elastin-labeled images were combined to obtain average behavior of the alveolar structure. The mean ± SD values of Ar at a strain of $\epsilon = 0$ were 0.95 ± 0.32, 0.99 ± 0.19, and 1.02 ± 0.41 in hypotonic, normal, and hypertonic solutions, respectively, not different from unity or each other. At $\epsilon = 0.3$, the Ar values were 1.16 ± 0.36, 1.26 ± 0.27, and 1.38 ± 0.44 in hypotonic, normal, and hypertonic solutions, respectively. Despite the large variability, the solution had a significant effect on Ar (1-way ANOVA, $P < 0.02$) and Ar increased linearly with osmolarity [Ar = (0.51 × osmolarity) + 1.16; $r^2 = 0.96$].

Modeling results. We created five different random networks with an SD of Ar of ~0.2 at $\epsilon = 0$ similar to that seen in the images. Figure 3 shows the average stress-strain curves for a variety of model parameters. In all simulations, the linear spring constant was fixed to $k = 1$. Each panel in Fig. 3 shows

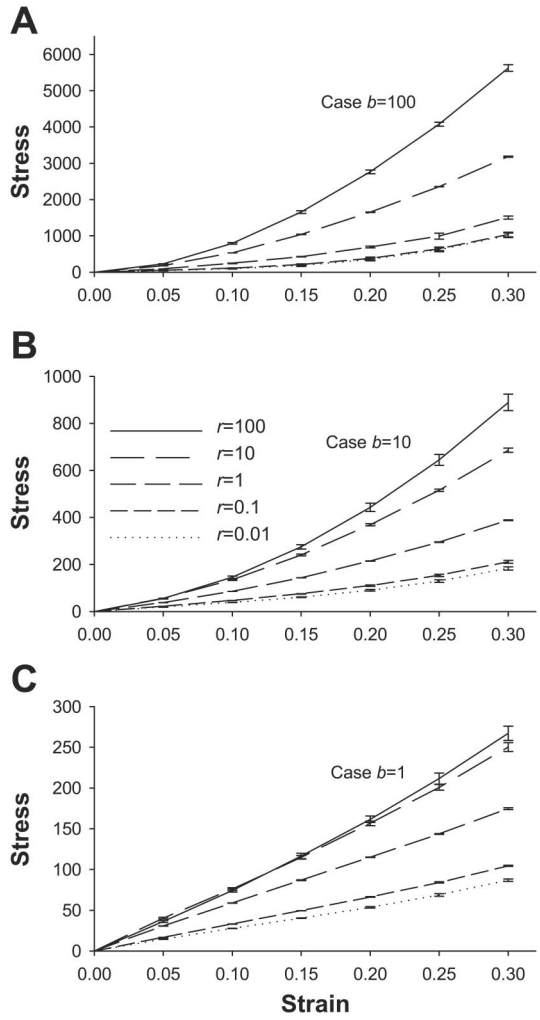

Fig. 3. Means ± SD of stress-strain curves from model simulations for nonlinear spring constant (b) values of 100 (A), 10 (B), and 1 (C) and for 5 values of the bond-bending constant (r). Stresses were averaged for 5 network configurations and are given in arbitrary units.

five stress-strain curves with the bond-bending constant r varied logarithmically from 0.01 to 100. Figure 3, *A–C*, corresponds to data obtained with the nonlinear spring constant b set to 100, 10, and 1, respectively. All curves were nonlinear, and the stress increased significantly with increasing r. The variability of the stress-strain curve due to different network configurations ranged between 2 and 15% of the stress depending on the parameter values. The maximum stress significantly increased with increasing b for any value of r. For $b = 1$, the stress-strain curves were essentially linear. Comparing these stress-strain curves with those in Fig. 1, it appears that a b/k ratio of 10 to 100 and a r/k ratio of 0.01 to 10 may be appropriate to account for the experimental data.

The configurations of a given network at $\epsilon = 0.3$ are compared for $r = 100$ (Fig. 4*A*) and $r = 0.01$ (Fig. 4*B*), mimicking stiff proteoglycans in hypotonic and soft proteoglycans in hypertonic solutions, respectively. When r was high (hypotonic case), the network stretched more by stretching the line elements. The individual springs were stretched more carrying higher energy, which resulted in a stiffer network with a more nonlinear stress-strain curve than in the low-r case. Alternatively, when r was small (hypertonic case), the network stretched primarily by changing the angles between two line elements. The transfer of energy and hence force follows nearly a straight path (red color) in the middle of the network. Additionally, because the angles are more conserved in the high-r case, line elements nearly perpendicular to ϵ were stretched and carried higher energy than in the low-r case. As a consequence, small islands of high energy appeared in the network (shown by red).

The microscopic Ar of the model depended greatly on how far Ar was evaluated from the left and right boundaries of the network. To compare Ar from the model and from imaging, Ar was evaluated in 25 hexagons in the center of the network, four rows and columns away from the boundaries. As shown in Fig. 5, the Ar decreased with r according to a sigmoidal curve on a semilog graph for all three values of b. For comparison, the mean values of the experimental Ar are also shown in Fig. 5. The range of r from 0.01 to 0.1 provided Ar values that were consistent with the proteoglycan stiffness in hypertonic solution, whereas the ranges of r from 1 to 10 and 10 to 100 were consistent with Ar values obtained in normal and hypotonic solutions, respectively.

DISCUSSION

To clarify the roles of elastin and collagen in lung mechanical properties, Setnikar (32) introduced the idea that elastin was responsible for maintaining tension at lower strains, whereas collagen contributed to the stress-strain properties at higher strains. Fukaya et al. (11) were the first to report stress-strain measurements on small lung tissue strips in vitro. Comparing their data to the known properties of elastic and collagen fibers, they argued that the mechanical properties of the alveolar walls are consistent with the so-called "nylon stocking effect" whereby individual elements are woven into a network and the response to stretching is essentially a network effect. Subsequently, many models have been proposed to link the micromechanical characteristics of the fiber network to the elastic properties of the lung using two-dimensional (21, 24, 37) and three-dimensional (7, 8) models. However, these models do not take into account the presence of ground substance or its interaction with the fiber network. Mijailovic et al. (25) reported similar macroscopic measurements to our data in fresh tissues. Their results may have been confounded by active cellular contraction, which we avoided by storing the tissue in a bath for 24 h, a period over which cellular contributions become negligible (39). Recently, Al Jamal et al. (1) studied the role of GAGs on the mechanical properties of lung tissue strips. Using a variety of GAG digesting enzymes, they found that, after a relatively long incubation time (3–16 h), the mechanical parameters describing stiffness of control samples generally decreased more than those of the digested samples. Interestingly, digestion of hyaluronic acid, a GAG not linked to a protein core, had minimal effects on mechanical properties. Among the GAGs, hyaluronic acid does not have sulfated side groups, and hence it has the smallest fixed charge density. Therefore, digesting hyaluronic acid should have little effect on tissue swelling. It is thus reasonable to conclude that it is the swelling of the charged GAGs on the proteoglycans that influences the macroscopic quasi-static mechanical properties of lung tissue strips.

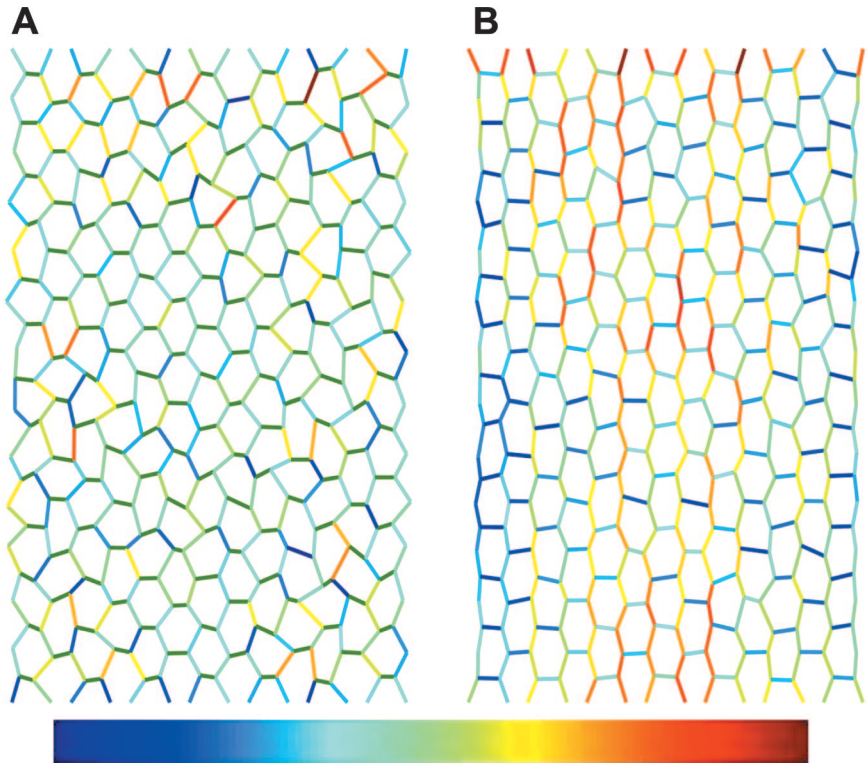

Fig. 4. Effects of the parameter r on the configuration of the elastic network model at 30% strain in the vertical direction. *A*: stiff network with $r = 100$. *B*: soft network with $r = 0.01$. Color is proportional to energy carried by the springs. The maximum energy values corresponding to dark red on *A* and *B* are different.

In a study by Lanir et al. (19), it was found that the swelling properties of proteoglycans in the myocardial soft tissue had a substantial effect on the residual strain characterized by the opening angle in radially cut equatorial cross-sectional slices of the heart. This is a mechanism that also generates bending rigidity of the tissue. Our results are consistent with those of Lanir et al. and suggest that the electromechanical properties of the proteoglycans significantly contribute to the quasi-static stress-strain curve of lung tissue. By increasing or decreasing the electrical repulsive forces in the GAGs, the proteoglycans become inflated or deflated, which shifts the stress-strain curve to the left or right, respectively. This hypothesis was supported by direct images of the distortion of the structure. We also developed a model of the fiber network that was able to reproduce the experimental stress-strain curves as well as to predict the microscopic distortion of the alveolar structure.

The primary assumption behind our interpretation of the data and modeling is that osmolarity has a major effect on the properties of the proteoglycans, but not on elastin or collagen, a well-accepted notion in the cartilage literature (4, 9, 15, 28). Unfortunately, such data for lung tissue do not exist. Nevertheless, we note the following. With regard to elastin, which is a hydrophobic molecule, the mechanical properties have been reported to be rather insensitive to changes in osmolarity (5). The effect of osmolarity on collagen is more complex because collagen has hydrophilic residues. The fixed-charge density of collagen was estimated to be about an order of magnitude smaller than that of the proteoglycans, and, as a consequence, collagen swells very little compared with proteoglycans, which in a dilute solution can occupy a domain as high as 1,000 times the volume of the chain in an unhydrated state (22). Indeed, the study by Fratzl and Daxer (10) suggests that during drying of corneal tissue the collagen interfibrillar distance decreases considerably primarily because of the presence of a proteoglycan coating layer surrounding the collagen, and this layer appears to form a complex three-dimensional fractal structure capable of collapsing or inflating depending on the osmolarity. At a critical dehydration point, the structure of the collagen also changes. However, at normal physiological hydration levels, it is only the interfibrillar space that changes dimensions because of loss or gain of water (10).

With regard to our data, we note that the difference in stress developed by the tissue in hypotonic and hypertonic solutions significantly decreased after amylase treatment, which hydrolyzes saccharide bonds and hence digests most GAGs. Because

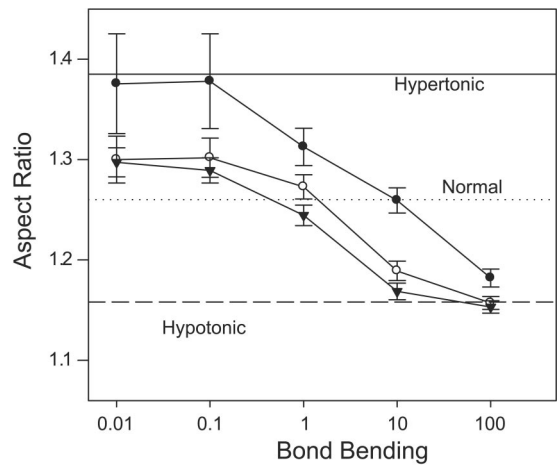

Fig. 5. Aspect ratio from the model as a function of bond bending for different nonlinear spring constants (●, $b = 100$; ○, $b = 10$; ▼, $b = 1$). Mean values of the aspect ratios from the experimental data are also displayed with straight lines (solid line, hypertonic; dotted line, normal; dashed line, hypotonic).

we did not measure what percent of the GAGs was actually digested by amylase, the residual difference in stress could be due to some leftover GAGs or potentially sensitivity of other matrix molecules to osmotic changes. Nevertheless, on the basis of the physical properties of elastin and collagen discussed above as well as our amylase experiments, it seems likely that most of the change in stress that developed in the lung tissue because of a change in osmolarity was substantially influenced by the state of swelling of the proteoglycans.

Model parameters. The model is composed of nonlinearly elastic line elements (*Eq. 1*) and linearly elastic bond-bending elements (*Eq. 2*). There is experimental evidence that a single collagen fiber behaves nonlinearly (35), which justifies the inclusion of a nonlinear line element. The stress-strain curves in Fig. 1, however, did not show a strong nonlinearity in the applied strain range. Therefore, we limited our analysis to the simplest form of nonlinearity, a second-order force-length relation, which is third order in terms of energy. With regard to *Eq. 2*, we note that cartilage has a reasonably linear stress-strain relation in compression primarily attributable to the charged proteoglycans (9). Thus, for simplicity, we chose a linear constitutive law for bond bending.

To interpret the parameters, we examine how the energy and stress scale with network size. If l_0 is the initial length and $\epsilon_s = \Delta l/l_0$ is the microscopic strain of the springs, the total energy of the network is obtained as the spring energy E_s (*Eq. 1*) and the angular energy E_a (*Eq. 2*) summed over all springs and nodes:

$$E = kl_0^2\left\{\frac{1}{2}\sum_{\text{springs}}\epsilon_s^2 + \frac{1}{3}\frac{bl_0}{k}\sum_{\text{springs}}\epsilon_s^3 + \frac{1}{2}\frac{r}{kl_0^2}\sum_{\text{nodes}}\Delta\theta^2\right\} \quad (3)$$

The goal is to express this sum as a product of the system size and a function that only depends on the average properties of the hexagons and the macroscopic strain ϵ. The number of springs N_s in the system is $\sim 3N_xN_y/2$ for large systems, where N_x and N_y are the number of nodes in the x and y directions, respectively. Thus *Eq. 3* can be written as

$$E = N_s kl_0^2\left\{\frac{1}{2}\langle\epsilon_s^2\rangle + \frac{1}{3}\frac{bl_0}{k}\langle\epsilon_s^3\rangle + \frac{1}{3}\frac{r}{kl_0^2}\langle\Delta\theta^2\rangle\right\} \quad (4)$$

where angle brackets denote averaging over the network when E is minimized. We confirmed the linear relation between N_s and E using various networks at $\epsilon = 0.3$ for N_s ranging from 32 to 7,426 with E averaged over five random configurations for each N_s. The stress σ can now be calculated by taking the derivative of the energy density (i.e., E per unit volume) with respect to ϵ. The volume of the system is $V = WLH$ where W is the width, L is the length, and H is the thickness of the sample. Because each factor is proportional to l_0, V is written as $V = C_1N_xN_yN_zl_0^3$, where N_z is the number of nodes in the z direction (for the simulations $N_z = 1$) and C_1 is a numerical constant of order 1. The N_s can be factored as $N_s = C_2N_xN_yN_z$, where C_2 is another constant. Substituting these into *Eq. 4*, the stress is given by

$$\sigma = C\frac{k}{l_0}\frac{\partial}{\partial\epsilon}S\left(\epsilon, \frac{bl_0}{k}, \frac{r}{kl_0^2}\right) \quad (5)$$

where $C = C_2/C_1$ and S is a dimensionless shape function that describes the average energy of a hexagon within the network, which allows us to replace ϵ_s by ϵ.

Equation 5 enables us to evaluate the model parameters from experimental data. For any combination of b/k and r/k, S specifies a unique stress-strain response of a single hexagon. Thus the ratio of the experimental stress and the simulated stress normalized to unit volume (i.e., by $N_s = 527$) should be independent of S and should scale with the ratio of k/l_0 obtained from the experiments and the simulations. By comparing the stress-strain curves (Figs. 1 and 3*B*) as well as Ar (Fig. 5) from the simulation and the experiments, we assume that $b = 10$ and $r = 5$ are reasonable values for describing the mechanics of the tissue in normal solution. Thus, dividing the experimental and the numerical stresses at $\epsilon = 0.3$ and using k/l_0 from the model and $l_0 = 40$ μm from the imaging (Fig. 2), we estimated that k for a single alveolar wall is 4×10^{-3} N/m.

The numerical value of k depends on the dimensions of the alveolar wall. The corresponding Young's modulus of the wall (Y_a) can be obtained by the scaling $Y_a = kl_0/A_0$, where A_0 is the cross-sectional area of the wall perpendicular to the focal plane. From our images, the average wall thickness was 8 μm. Because the walls are randomly oriented, the width of the wall resisting deformation is also equal to the length of the wall (40 μm) and hence $A_0 = 320$ μm^2, which gives $Y_a = 5$ kPa, which is 10 times larger than $Y = 0.5$ kPa for the entire tissue strip near $\epsilon = 0$ (Fig. 1).

The Y_a can also be related to the Young's modulus of a single collagen fiber in the alveolar wall. The Young's modulus of a fiber reinforced composite is $Y_a = vY_f + (1 - v)Y_m$ where Y_f and Y_m are the moduli of the fibers and the matrix, respectively, and v is the volume fraction of the fibers (15). As a first approximation, we neglect the contribution of the matrix (i.e., $Y_m = 0$). The average diameter of the collagen fibers is 1 μm (33). A line element in our images corresponds to a 8 μm × 40 μm rectangular slice of the alveolar wall. The higher magnification of collagen-labeled tissue in Fig. 6 shows significant heterogeneity with one to four wavy fibers embedded in the alveolar walls. Because the direction of this slice is

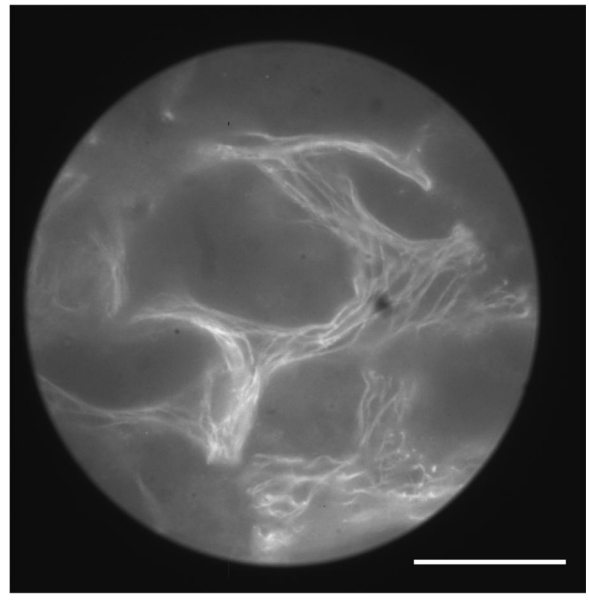

Fig. 6. Collagen-labeled unstretched tissue at a higher magnification. Note that wavy collagen fibers are running nearly parallel in the alveolar walls. Bar represents 50 μm.

random, v is estimated to be 0.08, which, from *Eq. 6*, corresponds to $Y_f = 63$ kPa. This value likely represents a lower bound for the following reasons. *1*) We used only the linear part of the spring constant in *Eq. 1*, and the moduli were evaluated at $\epsilon = 0$. Indeed, comparing the dimensionless quantity bl_0/k from *Eq. 5* from the model and the data, we obtained $b = 1.2$ kPa for the alveolar wall, which increases the apparent spring constant to 2×10^{-2} N/m $\epsilon = 0.3$. Hence, the corresponding estimate of the fiber modulus is $Y_f = 300$ kPa. *2*) The expression for Y_a is a gross oversimplification because it does not take into account the structure of the alveolar wall. *3*) The collagen fibers show a wide distribution of curvature (33). As a consequence, during uniaxial stretching, many fibers may first unfold and contribute to stress only at higher strains. Nevertheless, to our knowledge, these are the first modulus estimates of a single alveolar wall and a single collagen fiber in lung tissue. Values for the Young's modulus of a single collagen molecule have been reported to vary from 3 to 10 GPa (31). The modulus of collagen fibrils from tendon increases linearly with fibril diameter, with values ranging from 1 to 5 MPa at lower strains, but at higher strains the modulus becomes independent of diameter (6). The modulus is also a function of the type and amount of small proteoglycans within the fibers and the ultrastructure of the fiber (29). Because such information is not available for lung collagen fibers, direct comparison of the modulus to those obtained from tendon is not possible.

The bond-bending parameter r represents both the compressive and the shear resistance of the proteoglycan matrix against deformation. Because the actual deformation of the matrix is not known and the shear properties of the proteoglycans are much less studied (28), we limit our discussion to the compressibility of the matrix. To relate r to molecular parameters of the proteoglycan matrix, we first note that the bulk modulus of proteoglycans depends on many factors including the composition of the matrix, osmolarity, pH, temperature, etc. (28). The compressive modulus of cartilage, which is composed of mainly proteoglycans, decreases by about a factor of 2 when NaCl concentration increases from 0.15 to 0.45 M (4, 9), which is similar to our results. The implications are interesting. When r is high, islands of highly stressed regions appear in the network because the hexagons are unable to fold (Fig. 4*A*). These islands must be a consequence of the particular irregular geometry in the unstressed state because the elastic parameters of the model are homogenous throughout the system. Such behavior suggests that, as in other tissues (3), the deformation of the alveolar walls is not affine, which is also supported by direct observation of the folding pattern on our images. When r is reduced, the network is softer and the stress-strain curve shifts to the right (Fig. 3). At the same time, the network laterally contracts because the hexagons fold especially near the free boundaries. The folding is attenuated in the middle of the network, and force transfer occurs primarily along straight lines parallel to the strain in the middle of the network (Fig. 4*B*). Thus r can modify the macroscopic Poisson ratio of the lattice. Because the stress-strain curve is sensitive to the compressibility of the proteoglycans (Fig. 1), we conclude that proteoglycans contribute to the Poisson ratio of the lung tissue by affecting the stability of the fiber network, hence the stability of the alveoli at lower lung volumes.

Physiological implications. The intersample variability of the stress at a given strain in Fig. 1 reached 50%. The variability of stress from the model, which is related to the five different configurations used in the simulations, remained below 15%. Thus part of the variability of the data can be due to the heterogeneity of structure in the different samples. The additional variability may be related to the fact that the different tissue strips may contain different numbers of small and medium-sized airways (30). The effects of such large variations in structure on the stresses were not investigated.

The question arises as to what extent the elastin contributes to mechanics. If elastin and collagen were simply running in parallel within the alveolar wall, the stiff collagen would dominate the response and digesting elastin should have no effect on mechanics. Although digesting elastin does decrease the modulus, digesting collagen always provides a larger decrease in stiffness (38), which is in accord with the notion that the two networks are entangled and likely cross-linked. Additionally, collagen fibers have "crimps" along their axis that, during stretching, first unfold before the fiber stretches. In tendon, crimps completely unfold by 5% strain, below which collagen does not develop appreciable stress (27). Thus it appears that the network organization of collagen is a dominant factor in the elastic behavior of lung tissue. However, our studies also suggest that the interaction of the fibers with proteoglycans also contributes to mechanics because the proteolgycans influence the extent to which collagen fibers fold and stretch.

Stretching the tissue strips uniaxially amplifies the changes in angles between fibers compared with a uniform biaxial or an isotropic three-dimensional stretching. Thus our analysis may overestimate the role of proteoglycans during normal breathing. If a hexagonal network is homogeneous, there are no changes in angles during uniform biaxial loading and bond bending does not contribute to mechanics. However, our images show significant heterogeneity in alveolar wall length, angle, and width (Fig. 2). Thus the fibers constitute a sufficiently heterogeneous network for significant changes in angle to occur during an isotropic two-dimensional stretching. Moreover, in disease, there is ample evidence of excessive heterogeneity in the lung, which results in a high degree of nonuniform ventilation and stretching of the lung tissue in three dimensions as well (23).

In summary, we suggest a new mechanical role for the proteoglycan matrix: the compressibility of the proteoglycans contributes to the stability of the fiber network of the lung. We also introduce a network model that takes into account the microscopic interaction between the fibers and the matrix. The model allows us to span the scale from macroscopic tissue mechanics to the compressibility of the proteoglycan matrix and the elasticity of single collagen fibers.

GRANTS

This study was supported by National Institutes of Health Grant 59215-04.

REFERENCES

1. **Al Jamal R, Roughley PJ, and Ludwig MS.** Effect of glycosaminoglycan degradation on lung tissue viscoelasticity. *Am J Physiol Lung Cell Mol Physiol* 280: L306–L315, 2001.
2. **Arbabi S and Sahimi M.** Elastic properties of three-dimensional percolation networks with stretching and bond-bending forces. *Phys Rev B Condens Matter* 38: 7173–7176, 1988.

3. **Billiar KL and Sacks MS.** A method to quantify the fiber kinematics of planar tissues under biaxial stretch. *J Biomech* 30: 753–756, 1997.
4. **Buschmann MD and Grodzinsky AJ.** A molecular model of proteoglycan-associated electrostatic forces in cartilage mechanics. *J Biomech Eng* 117: 179–192, 1995.
5. **Chalmers GWG, Gosline JM, and Lillie MA.** The hydrophobicity of vertebrate elastin. *J Exp Biol* 202: 301–314, 1999.
6. **Christiansen DL, Huang EK, and Silver FH.** Assembly of type I collagen: fusion of fibril subunits and the influence of fibril diameter on mechanical properties. *Matrix Biol* 19: 409–420, 2000.
7. **Dale PJ, Matthews LF, and Schroter RC.** Finite element analysis of lung alveolus. *J Biomech* 13: 865–873, 1980.
8. **Denny E and Schroter RC.** The mechanical behavior of a mammalian lung alveolar duct model. *J Biomech Eng* 117: 254–261, 1995.
9. **Eisenberg SR and Grodzinski AJ.** Swelling of articular cartilage and other connective tissue: electromechanical forces. *J Orthop Res* 3: 148–159, 1985.
10. **Fratzl P and Daxer A.** Structural transformation of collagen fibrils in corneal stroma during drying. An x-ray study. *Biophys J* 64: 1210–1214, 1993.
11. **Fukaya H, Martin CJ, Young AC, and Katsura S.** The mechanical properties of the alveolar walls. *J Appl Physiol* 25: 689–695, 1968.
12. **Fung YC.** *Biomechanics: Mechanical Properties of Living Tissues*. New York: Springer-Verlag, 1981.
13. **Hulmes DJS, Wess TJ, Prockop DJ, and Fratzl P.** Radial packing, order, and disorder in collagen fibrils. *Biophys J* 68: 1661–1670, 1995.
14. **Ingenito EP, Mark L, and Davison B.** Effects of acute lung injury on dynamic tissue properties. *J Appl Physiol* 77: 2689–2697, 1994.
15. **Jeronimidis G and Vincent JFV.** Composite materials. In: *Connective Tissue Matrix*, edited by Hukins DWL. Weinheim: Verlag-Chemie, 1984, p. 187–210.
16. **Kamm RD.** Airway wall mechanics. *Annu Rev Biomed Eng* 1: 47–72, 1999.
17. **Karlinsky JB.** Stress-strain characteristics of normal and emphysematous hamster lung strips. *Respir Physiol* 90: 251–260, 1992.
18. **Kirkpatrick S, Gelatt CD, and Vecchi MP Jr.** Optimization by simulated annealing. *Science* 220: 671–680, 1983.
19. **Lanir Y, Hayam G, Abovsky M, Zlotnick AY, Uretzky G, Nevo E, and Ben-Haim SA.** Effect of myocardial swelling on residual strain in the left ventricle of the rat. *Am J Physiol Heart Circ Physiol* 270: H1736–H1743, 1996.
20. **Lewis JF and Jobe AH.** Surfactant and the adult respiratory distress syndrome. *Am Rev Respir Dis* 147: 218–233, 1993.
21. **Maksym GN, Fredberg JJ, and Bates JHT.** Force heterogeneity in a two-dimensional network model of lung tissue elasticity. *J Appl Physiol* 85: 1223–1229, 1998.
22. **Maroudas A and Bannon C.** Measurement of swelling pressure in cartilage and comparison with the osmotic pressure of constituent proteoglycans. *Biorheology* 18: 619–632, 1981.
23. **Martynowicz MA, Minor TA, Walters BJ, and Hubmayr RD.** Regional expansion of oleic acid-injured lungs. *Am J Respir Crit Care Med* 160: 250–258, 1999.
24. **Mead J, Takishima T, and Leith D.** Stress distribution in lungs: a model of pulmonary elasticity. *J Appl Physiol* 28: 596–608, 1970.
25. **Mijailovich SM, Stamenovic D, Brown R, Leith DE, and Fredberg JJ.** Dynamic moduli of rabbit lung tissue and pigeon ligamentum propatagiale undergoing uniaxial cyclic loading. *J Appl Physiol* 76: 773–782, 1994.
26. **Minns RJ, Soden PD, and Jackson DS.** The role of the fibrous components and ground substance in the mechanical properties of biological tissues: a preliminary investigation. *J Biomech* 6: 153–165, 1973.
27. **Misof K, Rapp G, and Fratzl P.** A new molecular model for collagen elasticity based on synchrotron X-ray scattering evidence. *Biophys J* 72: 1376–1381, 1997.
28. **Mow VC, Holmes MH, and Lai MW.** Fluid transport and mechanical properties of articular cartilage: a review. *J Biomech* 17: 377–394, 1984.
29. **Redaelli A, Vesentini S, Soncini M, Vena P, Mantero S, and Montevecchi FM.** Possible role of decorin glycosaminoglycans in fibril to fibril force transfer in relative mature tendons—a computational study from molecular to microstructural level. *J Biomech* 36: 1555–1569, 2003.
30. **Salerno FG, Dallaire M, and Ludwig MS.** Does the anatomic makeup of parenchymal lung strips affect oscillatory mechanics during induced constriction? *J Appl Physiol* 79: 66–72, 1995.
31. **Sasaki N and Odajima S.** Stress-strain curve and Young's modulus of a collagen molecule as determined by the X-ray diffraction technique. *J Biomech* 29: 655–658, 1996.
32. **Setnikar I.** Origin and significance of the mechanical property of the lung. *Arch Fisiol* 55: 349–374, 1955.
33. **Sobin SS, Fung YC, and Tremer HM.** Collagen and elastin fibers in human pulmonary alveolar walls. *J Appl Physiol* 64: 1659–1675, 1988.
34. **Stamenovic D.** Micromechanical foundations of pulmonary elasticity. *Physiol Rev* 70: 1117–1134, 1990.
35. **Stromberg DD and Wiederhielm CA.** Viscoelastic description of a collagenous tissue in simple elongation. *J Appl Physiol* 26: 857–862, 1969.
36. **Tang W and Thorpe MF.** Percolation of elastic networks under tension. *Phys Rev B Condens Matter* 37: 5539–5551, 1988.
37. **Wilson TA.** A continuum analysis of a two-dimensional mechanical model of the lung parenchyma. *J Appl Physiol* 33: 472–478, 1972.
38. **Yuan H, Kononov S, Cavalcante FSA, Lutchen KR, Ingenito EP, and Suki B.** Effects of collagenase and elastase on the mechanical properties of lung tissue strips. *J Appl Physiol* 89: 3–14, 2000.
39. **Yuan H, Ingenito EP, and Suki B.** Dynamic properties of lung parenchyma: mechanical contributions of fiber network and interstitial cells. *J Appl Physiol* 83: 1420–1431, 1997.